First Measurement of Coherent Elastic Neutrino-Nucleus Scattering on Argon

D. Akimov,[1,2] J. B. Albert,[3] P. An,[4,5] C. Awe,[4,5] P. S. Barbeau,[4,5] B. Becker,[6] V. Belov,[1,2] I. Bernardi,[6] M. A. Blackston,[7] L. Blokland,[6] A. Bolozdynya,[2] B. Cabrera-Palmer,[8] N. Chen,[9] D. Chernyak,[10] E. Conley,[4] R. L. Cooper,[11,12] J. Daughhetee,[6] M. del Valle Coello,[3] J. A. Detwiler,[9] M. R. Durand,[9] Y. Efremenko,[6,7] S. R. Elliott,[12] L. Fabris,[7] M. Febbraro,[7] W. Fox,[3] A. Galindo-Uribarri,[6,7] A. Gallo Rosso,[13] M. P. Green,[5,7,14] K. S. Hansen,[9] M. R. Heath,[7] S. Hedges,[4,5] M. Hughes,[3] T. Johnson,[4,5] M. Kaemingk,[11] L. J. Kaufman,[3,†] A. Khromov,[2] A. Konovalov,[1,2] E. Kozlova,[1,2] A. Kumpan,[2] L. Li,[4,5] J. T. Librande,[9] J. M. Link,[15] J. Liu,[10] K. Mann,[5,7] D. M. Markoff,[5,16] O. McGoldrick,[9] H. Moreno,[11] P. E. Mueller,[7] J. Newby,[7] D. S. Parno,[17] S. Penttila,[7] D. Pershey,[4] D. Radford,[7] R. Rapp,[17] H. Ray,[18] J. Raybern,[4] O. Razuvaeva,[1,2] D. Reyna,[8] G. C. Rich,[19] D. Rudik,[1,2] J. Runge,[4,5] D. J. Salvat,[3] K. Scholberg,[4] A. Shakirov,[2] G. Simakov,[1,2,20] G. Sinev,[4] W. M. Snow,[3] V. Sosnovtsev,[2] B. Suh,[3] R. Tayloe,[3,*] K. Tellez-Giron-Flores,[15] R. T. Thornton,[3,12] I. Tolstukhin,[3,‡] J. Vanderwerp,[3] R. L. Varner,[7] C. J. Virtue,[13] G. Visser,[3] C. Wiseman,[9] T. Wongjirad,[21] J. Yang,[21] Y.-R. Yen,[17] J. Yoo,[22,23] C.-H. Yu,[7] and J. Zettlemoyer[3]

(COHERENT Collaboration)

[1]*Institute for Theoretical and Experimental Physics named by A. I. Alikhanov of National Research Centre "Kurchatov Institute," Moscow, 117218, Russian Federation*
[2]*National Research Nuclear University MEPhI (Moscow Engineering Physics Institute), Moscow, 115409, Russian Federation*
[3]*Department of Physics, Indiana University, Bloomington, Indiana 47405, USA*
[4]*Department of Physics, Duke University, Durham, North Carolina 27708, USA*
[5]*Triangle Universities Nuclear Laboratory, Durham, North Carolina 27708, USA*
[6]*Department of Physics and Astronomy, University of Tennessee, Knoxville, Tennessee 37996, USA*
[7]*Oak Ridge National Laboratory, Oak Ridge, Tennessee 37831, USA*
[8]*Sandia National Laboratories, Livermore, California 94550, USA*
[9]*Center for Experimental Nuclear Physics and Astrophysics and Department of Physics, University of Washington, Seattle, Washington 98195, USA*
[10]*Physics Department, University of South Dakota, Vermillion, South Dakota 57069, USA*
[11]*Department of Physics, New Mexico State University, Las Cruces, New Mexico 88003, USA*
[12]*Los Alamos National Laboratory, Los Alamos, New Mexico 87545, USA*
[13]*Department of Physics, Laurentian University, Sudbury, Ontario P3E 2C6, Canada*
[14]*Department of Physics, North Carolina State University, Raleigh, North Carolina 27695, USA*
[15]*Center for Neutrino Physics, Virginia Tech, Blacksburg, Virginia 24061, USA*
[16]*Department of Mathematics and Physics, North Carolina Central University, Durham, North Carolina 27707, USA*
[17]*Department of Physics, Carnegie Mellon University, Pittsburgh, Pennsylvania 15213, USA*
[18]*Department of Physics, University of Florida, Gainesville, Florida 32611, USA*
[19]*Enrico Fermi Institute and Kavli Institute for Cosmological Physics, University of Chicago, Chicago, Illinois 60637, USA*
[20]*Moscow Institute of Physics and Technology, Dolgoprudny, Moscow Region 141700, Russian Federation*
[21]*Department of Physics and Astronomy, Tufts University, Medford, Massachusetts 02155, USA*
[22]*Department of Physics at Korea Advanced Institute of Science and Technology (KAIST), Daejeon, 34051, Republic of Korea*
[23]*Institute for Basic Science (IBS), Daejeon, 34051, Republic of Korea*

We report the first measurement of coherent elastic neutrino-nucleus scattering (CEvNS) on argon using a liquid argon detector at the Oak Ridge National Laboratory Spallation Neutron Source. Two independent analyses prefer CEvNS over the background-only null hypothesis with greater than 3σ significance. The measured cross section, averaged over the incident neutrino flux, is $(2.2 \pm 0.7) \times 10^{-39}$ cm^2—consistent with the standard model prediction. The neutron-number dependence of this result, together with that from our previous measurement on CsI, confirms the existence of the CEvNS process and provides improved constraints on nonstandard neutrino interactions.

Introduction.—Coherent elastic neutrino-nucleus scattering (CEvNS) [1,2] occurs when a neutrino interacts coherently with the total weak nuclear charge, necessarily at low-momentum transfer, leaving the ground-state nucleus to recoil elastically. It is the dominant interaction for neutrinos of energy $E_\nu \lesssim 100$ MeV and provides a sensitive test of standard model (SM) and beyond-SM processes [3–6].

In this Letter, we report the first measurement of CEvNS in a light nucleus (argon) complementing our earlier result on cesium and iodine [7], thus establishing the N^2 behavior predicted by the standard model. This result also improves constraints on nonstandard interactions between neutrinos and quarks.

CEvNS is sensitive to these nonstandard interactions (NSIs), which are crucial to understand for the success of the long-baseline neutrino oscillation program [8–11]. The process also probes the weak nuclear charge [12–17] and the weak mixing angle at novel momentum transfer [6,18]. Additionally, CEvNS-sensitive detectors could play future roles as nonintrusive nuclear reactor monitors [19–21].

CEvNS has numerous connections to possible hidden-sector particles. It is sensitive to Z' models, which could explain the theoretical tension with measurements of the muon anomalous magnetic moment [22]. CEvNS from solar and atmospheric neutrinos constitute the so-called neutrino floor background in future dark matter searches [23], and CEvNS cross section measurements quantify this background. CEvNS experiments at accelerators are also sensitive to sub-GeV accelerator-produced dark matter particle models [24–28]. The potential relevance of CEvNS to core-collapse supernovae was quickly recognized [29], and though its role in supernova dynamics is uncertain [30,31], CEvNS is expected to be the source of neutrino opacity in these events [32]. Supernova neutrinos convey information about supernova dynamics and could be detected via CEvNS [33].

CEvNS measurements require detectors with low-nuclear-recoil-energy threshold in a low-background environment with an intense neutrino flux. The COHERENT Collaboration has deployed a suite of detectors in a dedicated neutrino laboratory ("Neutrino Alley") at the Spallation Neutron Source (SNS) at Oak Ridge National Laboratory [7,34]. We reported the first observation of CEvNS on heavy nuclei using a 14.6-kg, low-background, low-threshold CsI[Na] detector located 19.3 m from the SNS target [7].

As part of the COHERENT program, we deployed the 24-kg active-mass liquid-argon (LAr) CENNS-10 scintillator detector (Fig. 1) in Neutrino Alley to detect CEvNS in a light nucleus. The initial CENNS-10 deployment set a limit on the CEvNS cross section for argon and quantified backgrounds [35]. A subsequent upgrade provided a lower energy threshold with an eightfold improvement in light collection efficiency.
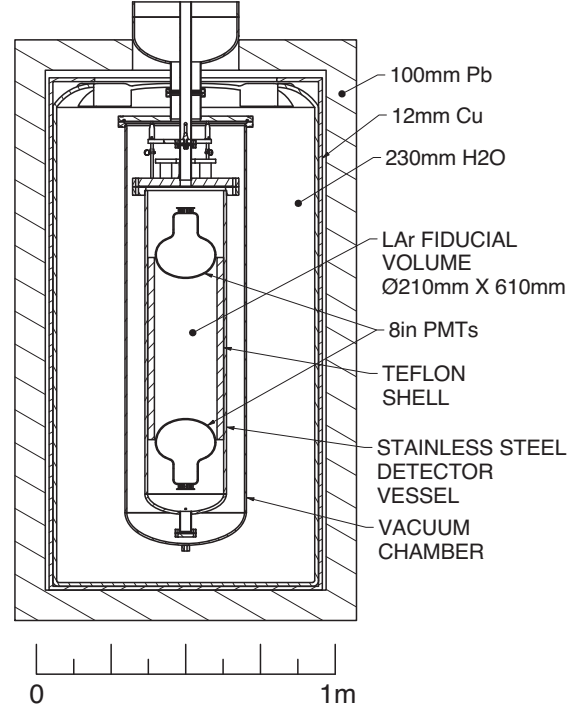

FIG. 1. CENNS-10 liquid argon detector and associated shielding as configured for the results reported here.

Experiment.—The 1-GeV, 1.4-MW proton beam of the SNS accelerator strikes a liquid-Hg target in 360 ns FWHM pulses at 60 Hz to produce neutrons that are moderated and delivered to experiments. Additionally, $(9.0 \pm 0.9) \times 10^{-2}$ π^+ are produced for each proton-on-target (POT) leading to a large flux of pion-decay-at-rest neutrinos. The π^+ produce a prompt 29.8 MeV ν_μ along with a μ^+, which subsequently decays yielding a three-body spectrum of $\bar{\nu}_\mu$ and ν_e with an endpoint energy of 52.8 MeV. This time structure is convolved with the proton beam pulse yielding a prompt ν_μ neutrino flux followed by a delayed flux of $\bar{\nu}_\mu$ and ν_e [7,34].

The CENNS-10 detector, designed and built at Fermilab [36], sits 27.5 m from the SNS target in Neutrino Alley. The active volume of CENNS-10 is defined by a cylindrical polytetrafluoroethylene (PTFE) shell and two 8-in. Hamamatsu R5912-02MOD photomultiplier tubes (PMTs) resulting in active mass of 24 kg of atmospheric argon (99.6% ^{40}Ar). The PTFE and PMT glass are coated with a 0.2 mg/cm^2 layer of 1,1,4,4-tetraphenyl-1,3-butadiene (TPB) to wavelength shift the 128-nm argon scintillation light to a distribution peaked at 420 nm, where the PMTs have quantum efficiency of 18%. This configuration provides a ~20 keVnr (nuclear-recoil) energy threshold.

Argon scintillation light from particle interactions is produced from both "fast" singlet ($\tau_s \approx 6$ ns) and "slow" triplet ($\tau_t \approx 1600$ ns) excited molecular states [37]. Electron recoils (ERs) and argon nuclear recoils (NRs) populate these states in different proportions, allowing for

pulse-shape discrimination (PSD) to suppress ER backgrounds from electron-gamma background sources compared to the CEvNS NR recoil signal. Neutron sources, from the accelerator or surrounding materials, will also create a NR signal, so shielding is required to reduce this background.

During SNS operation, each PMT waveform is digitized at 250 MHz in a 33-μs window around each POT pulse ("on-beam" data) together with a subsequent 33-μs window between POT pulses ("off-beam" data) to allow a measure of beam-unrelated backgrounds. Calibration data were acquired using ^{57}Co and ^{241}Am sources placed within the water shield, a sample of ^{83m}Kr gas injected via the argon recirculation system [38], as well as an external americium-beryllium (AmBe) neutron source. A pulsed visible-spectrum light-emitting diode (LED), along with triplet light from low-light-yield calibration pulses, was used to determine the response of the PMTs to single-photoelectron (SPE) signals. These calibration runs were performed on a weekly basis to correct for drifts in detector response due to PMT gain or light output changes.

Analysis.—In order to avoid experimenter bias, the analysis methods and event selection criteria were established, prior to examining the on-beam dataset, by two independent analysis groups labeled as "A" and "B" below.

The PMT waveforms were integrated over a 6-μs window after the initial PMT pulse and summed to form the integrated event amplitude I. Also, the integrated amplitude in the first 90 ns, I_{90}, was calculated and the PSD parameter $F_{90} = I_{90}/I$ defined. Off- and on-beam windows were treated identically, providing an unbiased measurement of the beam-unrelated backgrounds. The γ-ray sources were used to calibrate scintillation yield to electron-equivalent energy (keVee) with 2% uncertainty. The energy resolution was 9% at the 41.5 keVee ^{83m}Kr line. A comparison of the calibration source signals to SPE signals from a pulsed LED and from delayed low-light-yield events resulted in an estimated ~4.5 photoelectrons (PEs) per keVee.

The detector response to CEvNS NR events compared to calibration ER events is quantified via the so-called quenching factor (QF). We performed a linear fit to the world data [39–42] for QF on argon in the energy range 0–125 keVnr following the Particle Data Group prescription for combining measurements [43], incorporating the correlated uncertainties reported in Ref. [42]. With this fit and the ER calibration from above, the response to CEvNS NR events can be simulated. At 20 keVnr, the fit yields QF = 0.26 ± 0.01. The AmBe neutron source data were used to determine the PSD response for NR events via the use of the quantity F_{90} with energy dependence consistent with other measurements in LAr [37,44].

A GEANT4-based [45] program modeled the detector response for both CEvNS and neutron events to determine the CEvNS detection efficiency and construct predicted event distributions. The program simulates the production and quenching of LAr scintillation light, TPB absorption and reemission, and propagation of optical photons to the PMTs. The material optical parameters and LAr scintillation properties were adjusted to reproduce the calibration data and then used to estimate the CEvNS response and detection efficiency.

The beam-unrelated steady-state (SS) background was measured *in situ* using the off-beam triggers occurring one-for-one with on-beam triggers. The time window within the off-beam trigger can be made larger that the on-beam time window, allowing for an "oversampling" of the background, thus reducing the systematic uncertainty on the measured rate to < 1%. In addition, the energy and F_{90} distributions are also precisely measured, eliminating the need for knowledge of the exact source of this background and for any additional systematic errors. Qualitatively, the measured spectrum is consistent with a dominant background from the 565 keVee end point β decay of ^{39}Ar in the detector volume. The remainder is mostly from γ rays from surrounding materials or a nearby SNS target radioactive gas exhaust pipe, which are suppressed by the Pb shielding. Relative to the on-beam signal, these backgrounds are ~10^4-fold suppressed due to the pulsed SNS beam structure and ~10^2-fold further suppressed by PSD in the event selection.

The beam-related background events are caused by neutrons originating in the SNS target that elastically scatter in the argon, producing a NR event. Though this beam-related neutron (BRN) rate is highly suppressed in Neutrino Alley, the events occur in time with the beam, and the rate competes with the CEvNS rate in the detector. The BRN flux at the CENNS-10 location was measured with the SciBath neutron detector [46,47] in 2015, was further studied with the CENNS-10 engineering run [35], and was measured as part of this analysis in a three-week (0.54 GW hr) "no-water" run, in which the water shielding around the detector was drained. Neutrino-induced neutrons from neutrino interactions in the lead shielding [48] can also produce prompt NR events; however, the water shielding between the lead and detector reduces their contribution to <1 event in this dataset.

The data used for this CEvNS analysis correspond to total integrated beam power of 6.12 GW hr (13.7×10^{22} POT) collected between July 2017 and December 2018. Events are selected from both on- and off-beam datasets with identical cuts. Candidate events are initiated by requiring pulses with ≥ 2 PEs in both PMTs occurring within 20 ns of each other. This cut largely determines the energy threshold and rejects 15% of the predicted CEvNS events at lowest recoil energies. Pulses within an event must not exhibit preceding or delayed "pileup" pulses, rejecting a further 4% of events. In addition, analysis B required that each PMT recorded at least 20% of the total light in an event, reducing some background events that

TABLE I. Summary of parameters, errors, and results for the maximum-likelihood fit and cross section extraction. Analysis A divides the BRN component into "prompt" and "delayed" parts. "BRN" and "SS" are the beam-related-neutron and steady-state backgrounds.

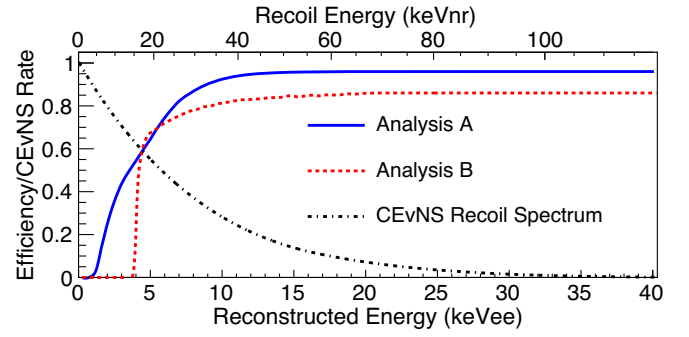| Analysis parameter	Analysis A	Analysis B
Fit ranges:		
F_{90}	0.5–0.9	0.5–0.8
E (keVee)	0.0–120.0	4.1–30.6
t_{trig} (μs)	−0.1–4.9	−1.0–8.0
Total events selected	3752	1466
Input values:		
N_{CEvNS}	128 ± 17	
N_{BRN}, prompt	497 ± 160	101 ± 12
N_{BRN}, delayed	33 ± 33	226 ± 33
N_{SS}	3152 ± 25	1155 ± 45
Total events predicted	3779	1482
Fit values:		
N_{CEvNS}	159 ± 43	121 ± 36
N_{BRN}, prompt	553 ± 34	222 ± 23
N_{BRN}, delayed	10 ± 11	
N_{SS}	3131 ± 23	1112 ± 41
Total events fit	3853	1455
Fit systematic errors:		
CEvNS F_{90} E dependence	4.5%	3.1%
CEvNS t_{trig} mean	2.7%	6.3%
BRN E distribution	5.8%	5.2%
BRN t_{trig} mean	1.3%	5.3%
BRN t_{trig} width	3.1%	7.7%
Total CEvNS sys. error	8.5%	13%
Fit results:		
Null significance (stat. only)	3.9σ	3.4σ
Null significance (stat.+sys.)	3.5σ	3.1σ
Cross section		
SM-predicted σ ($\times 10^{-39}$ cm^2)		1.8
Systematic errors:		
Detector efficiency	3.6%	1.6%
Energy calibration	0.8%	4.6%
F_{90} calibration	7.8%	3.3%
Quenching factor	1.0%	1.0%
Nuclear form factor	2.0%	2.0%
Neutrino flux	10%	10%
Total cross section sys. error	13%	12%
Measured σ ($\times 10^{-39}$ cm^2)	2.3 ± 0.7	2.2 ± 0.8

FIG. 2. Energy-dependent CEvNS event efficiency for analyses A (blue) and B (red dash) along with the predicted CEvNS recoil spectrum in arbitrary units (black dash-dotted line). Analysis B requires $E > 4.1$ keVee, as well as a "top-fraction" cut (see text).

analyses A and B because of different strategies for signal and background optimization. For example, analysis A used a wider energy range to include more high-energy BRN events to anchor that background, so an extra delayed-BRN component would be better constrained. The resulting energy-dependent efficiency for detecting CEvNS is shown in Fig. 2.

For the extraction of CEvNS events amid BRN and SS backgrounds, we performed an extended maximum-likelihood fit to the on-beam data binned in F_{90}, t_{trig}, and E. These data were modeled by distributions $\mathcal{P}_k(E, t_{\text{trig}}, F_{90})$ with associated number of events N_k for $k \in \{\text{CEvNS}, \text{BRN}, \text{SS}\}$. The best-fit number of CEvNS events, N_{CEvNS}, was unconstrained in the fit. $\mathcal{P}_{\text{CEvNS}}$ was determined from a simulation of CEvNS events to provide the PSD and energy distributions, then combining with the neutrino arrival-time dependence.

For the backgrounds, the total number of SS events N_{SS} was Gaussian constrained by the statistical error from the off-beam measurement of 0.8% (3.8%) for analysis A (B). The $\mathcal{P}_{\text{SS}}$ distribution was formed by binning the off-beam events in E and F_{90} and assuming a constant time dependence. Analysis A Gaussian-constrained N_{BRN} based on associated BRN measurements; analysis B allowed N_{BRN} to float freely. Analysis A also included a separate delayed ($1.4 < t_{\text{trig}} < 1.9$ μs) BRN component in the fit to permit the possibility of late BRN events. For $\mathcal{P}_{\text{BRN}}$, the F_{90}-E dependence was extracted from the simulation with a time dependence extracted from a fit to the no-water data.

Pseudodatasets were generated using RooFit [49] to demonstrate a robust and unbiased fitting procedure and to estimate uncertainties before fitting the on-beam data. Only systematic uncertainties that affect the shape of the $\mathcal{P}_k$ affect the fit value of N_{CEvNS}. The individual contributions are treated as independent and added in quadrature for the total systematic error on the fit number of CEvNS events.

Results.—The input parameters, errors, and results for the maximum likelihood fit of N_{CEvNS} for both analyses are summarized in Table I. The significance of this result

occur near either PMT, while reducing the CEvNS event selection efficiency by 10%.

Further, candidate events were required to lie in the F_{90} NR band to reject ER- and Cherenkov-like events. A time range was chosen using t_{trig}, where $t_{\text{trig}} = 0$ is the expected start time of the neutrino beam at the detector, to include both prompt and delayed neutrinos. An energy range was chosen to include the region** of interest for a CEvNS signal ($E < 120$ keVnr ≈ 30 keVee). The specific values for the fit ranges, summarized in Table I, differed between
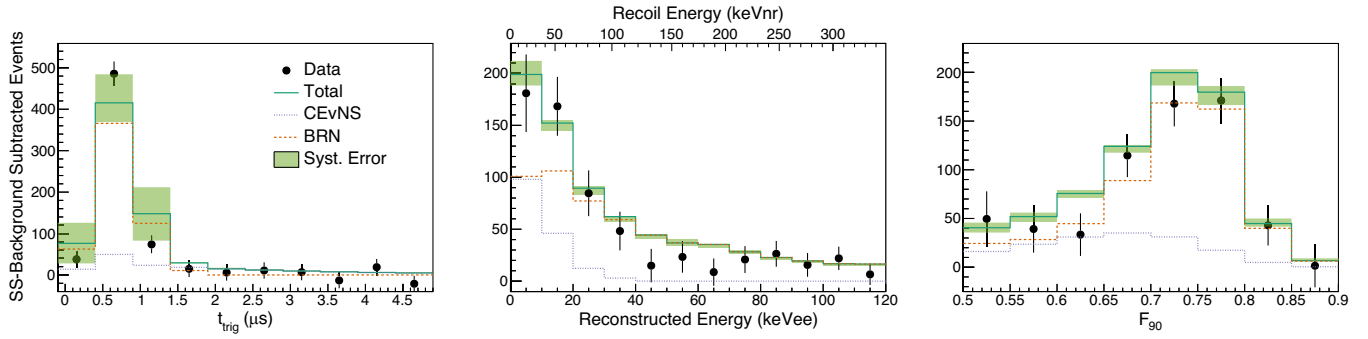
FIG. 3. Projection of the best-fit maximum likelihood probability density function (PDF) from analysis A on t_{trig} (left), reconstructed energy (center), and F_{90} (right) along with selected data and statistical errors. The fit SS background has been subtracted to better show the CEvNS component. The green band shows the envelope of fit results resulting from the $\pm 1\sigma$ systematic errors on the PDF.

compared to the null hypothesis, incorporating systematic errors as explained above, is 3.5σ (3.1σ) for analysis A (B). Both analyses yield N_{CEvNS} within 1σ of the SM prediction. Note that the large SS background is not as detrimental to signal significance as expected with a simple signal to background argument because it is well measured and of different character than signal in the $\mathcal{P}_k(E, t_{trig}, F_{90})$ distributions.

The data and best fit for analysis A are shown in Fig. 3, projected along E, F_{90}, and t_{trig}. Extraction of the relatively low-energy CEvNS signal is robust in the presence of the large prompt BRN background because of the latter's much harder spectrum.

We compute the CEvNS flux-averaged cross section on argon (99.6% ^{40}Ar) from the ratio of the best-fit N_{CEvNS} to that predicted by the simulation using the SM prediction of

1.8×10^{-39} cm^2. This incorporates the total uncertainty on the fit N_{CEvNS} along with additional systematic uncertainties, dominated by the 10% incident neutrino flux uncertainty, that do not affect the signal significance. The values are summarized along with extracted cross section values in Table I. The measured flux-averaged cross sections are consistent between the two analyses and with the SM prediction as shown in Fig. 4. We average the results of the two analyses to obtain $(2.2 \pm 0.7) \times 10^{-39}$ cm^2 with uncertainty dominated by the $\sim$30% statistical uncertainty on N_{CEvNS}.

This result is used to constrain neutrino-quark NSIs mediated by a new heavy vector particle using the framework developed in Refs. [3,10]. Here we consider the particular case of nonzero vectorlike quark-ν_e NSI
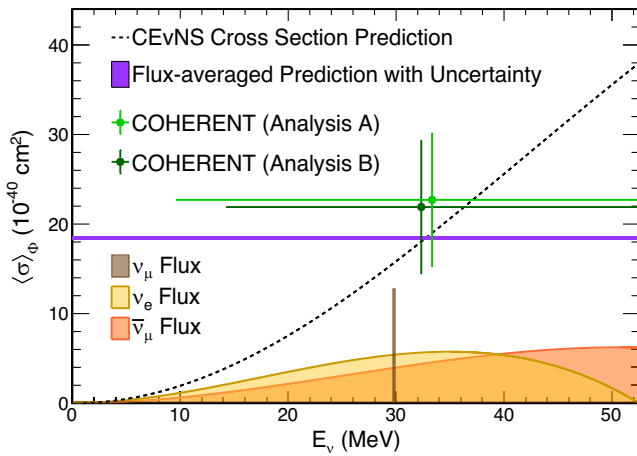

FIG. 4. Measured CEvNS flux-averaged cross section for the two analyses, along with the SM prediction. The horizontal bars indicate the energy range of the flux contributing. The minimum value is set by the NR threshold energy and is different for each analysis. The 2% error on the theoretical cross section due to uncertainty in the nuclear form factor is also illustrated by the width of the band. The SNS neutrino flux is shown with arbitrary normalization.
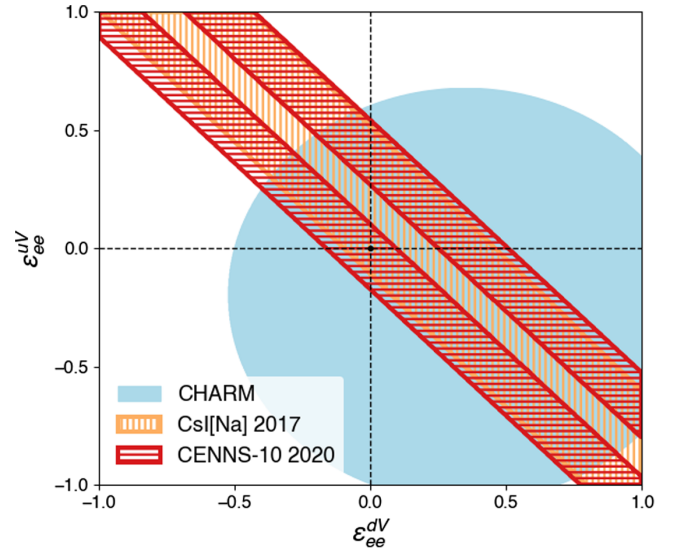

FIG. 5. 90% C.L. regions for nonstandard NSIs for a vector-coupled quark-electron interaction extracted from this argon measurement plotted together with the previous COHERENT CsI[Na] measurement [7] and the CHARM experiment [51]. The three regions shown are independent and the dashed black lines show the SM prediction.

couplings, ϵ_{ee}^{uV} and ϵ_{ee}^{dV}, as these two are the least experimentally constrained. The other couplings in this framework [9] are assumed to be zero. A comparison of the measured CEvNS cross section reported here to the predicted cross section including these couplings is used to determine the 90% C.L. (1.65σ) regions of NSI parameters as shown in Fig. 5. The same procedure was separately applied using our previous CsI[Na] result [7] and also plotted in Fig. 5. The Ar measurement, with a slight excess over the SM prediction, favors a slightly different region than CsI[Na] and results in a bifurcated region because the central area corresponds to values of ϵ_{ee}^{uV} and ϵ_{ee}^{dV} that yield a cross section somewhat less than the SM value. The data and predicted background are available [50] for alternative fits.

Summary.—A 13.7×10^{22} protons-on-target sample of data, collected with the CENNS-10 detector in the SNS Neutrino Alley at 27.5 m from the neutron production target, was analyzed to measure the CEvNS process on argon. Two independent analyses observed a more than 3σ excess over background, resulting in the first detection of CEvNS in argon. We measure a flux-averaged cross section of $(2.2 \pm 0.7) \times 10^{-39}$ cm^2 averaged over and consistent between the two analyses. This is the second, and much lighter, nucleus for which CEvNS has been measured, verifying the expected neutron-number dependence of the cross section and improving constraints on nonstandard neutrino interactions. CENNS-10 is collecting additional data, which will provide, along with refined background measurements, more precise results in the near future.

*rtayloe@indiana.edu
†SLAC National Accelerator Laboratory, Menlo Park, California 94205, USA.
‡Argonne National Laboratory, Argonne, Illinois 60439, USA.

[1] D. Freedman, Phys. Rev. D **9**, 1389 (1974).
[2] V. B. Kopeliovich and L. L. Frankfurt, Pis'ma Zh. Eksp. Teor. Fiz. **19**, 236 (1974) [JETP Lett. **19**, 145 (1974)].
[3] J. Barranco, O. G. Miranda, and T. I. Rashba, J. High Energy Phys. 12 (2005) 021.
[4] J. Barranco, O. G. Miranda, and T. I. Rashba, Phys. Rev. D **76**, 073008 (2007).
[5] B. Dutta, R. Mahapatra, L. E. Strigari, and J. W. Walker, Phys. Rev. D **93**, 013015 (2016).
[6] L. M. Krauss, Phys. Lett. B **269**, 407 (1991).
[7] D. Akimov *et al.* (COHERENT Collaboration), Science **357**, 1123 (2017).
[8] P. Coloma and T. Schwetz, Phys. Rev. D **94**, 055005 (2016); **95**, 079903(E) (2017).
[9] P. Coloma, P. B. Denton, M. C. Gonzalez-Garcia, M. Maltoni, and T. Schwetz, J. High Energy Phys. 04 (2017) 116.
[10] P. Coloma, M. C. Gonzalez-Garcia, M. Maltoni, and T. Schwetz, Phys. Rev. D **96**, 115007 (2017).
[11] J. Liao, D. Marfatia, and K. Whisnant, Phys. Rev. D **93**, 093016 (2016).
[12] P. S. Amanik and G. C. McLaughlin, J. Phys. G **36**, 015105 (2009).
[13] M. Cadeddu and F. Dordei, Phys. Rev. D **99**, 033010 (2019).
[14] K. Patton, J. Engel, G. C. McLaughlin, and N. Schunck, Phys. Rev. C **86**, 024612 (2012).
[15] M. Cadeddu, C. Giunti, Y. F. Li, and Y. Y. Zhang, Phys. Rev. Lett. **120**, 072501 (2018).
[16] D. A. Sierra, J. Liao, and D. Marfatia, J. High Energy Phys. 06 (2019) 141.
[17] M. Hoferichter, P. Klos, J. Menéndez, and A. Schwenk, Phys. Rev. D **99**, 055031 (2019).
[18] B. C. Cañas, E. A. Garcés, O. G. Miranda, and A. Parada, Phys. Lett. B **784**, 159 (2018).
[19] P. S. Barbeau, J. I. Collar, J. Miyamoto, and I. Shipsey, IEEE Trans. Nucl. Sci. **50**, 1285 (2003).
[20] C. Hagmann and A. Bernstein, IEEE Trans. Nucl. Sci. **51**, 2151 (2004).
[21] Y. Kim, Nucl. Eng. Technol. **48**, 285 (2016).

[22] H. Davoudiasl, H.-S. Lee, and W. J. Marciano, Phys. Rev. D **89**, 095006 (2014).

[23] M. C. Gonzalez-Garcia, M. Maltoni, Y. F. Perez-Gonzalez, and R. Z. Funchal, J. High Energy Phys. 07 (2018) 019.

[24] P. deNiverville, M. Pospelov, and A. Ritz, Phys. Rev. D **92**, 095005 (2015).

[25] S.-F. Ge and I. M. Shoemaker, J. High Energy Phys. 11 (2018) 066.

[26] B. Dutta, D. Kim, S. Liao, J.-C. Park, S. Shin, and L. E. Strigari, Phys. Rev. Lett. **124**, 121802 (2020).

[27] B. Dutta, S. Ghosh, and J. Kumar, Phys. Rev. D **100**, 075028 (2019).

[28] D. Akimov et al. (COHERENT Collaboration), Phys. Rev. D **102**, 052007 (2020).

[29] D. Z. Freedman, D. N. Schramm, and D. L. Tubbs, Annu. Rev. Nucl. Sci. **27**, 167 (1977).

[30] H.-T. Janka, Annu. Rev. Nucl. Part. Sci. **62**, 407 (2012).

[31] K. Balasi, K. Langanke, and G. Martínez-Pinedo, Prog. Part. Nucl. Phys. **85**, 33 (2015).

[32] S. W. Bruenn and A. Mezzacappa, Phys. Rev. D **56**, 7529 (1997).

[33] C. J. Horowitz, K. J. Coakley, and D. N. McKinsey, Phys. Rev. D **68**, 023005 (2003).

[34] D. Akimov et al. (COHERENT Collaboration), arXiv:1803.09183.

[35] D. Akimov et al. (COHERENT Collaboration), Phys. Rev. D **100**, 115020 (2019).

[36] S. J. Brice et al., Phys. Rev. D **89**, 072004 (2014).

[37] A. Hitachi, T. Takahashi, N. Funayama, K. Masuda, J. Kikuchi, and T. Doke, Phys. Rev. B **27**, 5279 (1983).

[38] D. Akimov et al. (COHERENT Collaboration), arXiv:2010.11258.

[39] P. Agnes et al., Phys. Rev. D **97**, 112005 (2018).

[40] H. Cao et al. (SCENE Collaboration), Phys. Rev. D **91**, 092007 (2015).

[41] W. Creus, Y. Allkofer, C. Amsler, A. D. Ferella, J. Rochet, L. Scotto-Lavina, and M. Walter, J. Instrum. **10**, P08002 (2015).

[42] D. Gastler, E. Kearns, A. Hime, L. C. Stonehill, S. Seibert, J. Klein, W. H. Lippincott, D. N. McKinsey, and J. A. Nikkel, Phys. Rev. C **85**, 065811 (2012).

[43] M. Tanabashi et al. (Particle Data Group), Phys. Rev. D **98**, 030001 (2018).

[44] C. Regenfus, Y. Allkofer, C. Amsler, W. Creus, A. Ferella, J. Rochet, and M. Walter, J. Phys. Conf. Ser. **375**, 012019 (2012).

[45] S. Agostinelli et al. (GEANT4 Collaboration), Nucl. Instrum. Methods Phys. Res., Sect. A **506**, 250 (2003).

[46] R. Tayloe, H. Meyer, D. Cox, J. Doskow, A. Ferguson, T. Katori, M. Novak, and D. Passmore, Nucl. Instrum. Methods Phys. Res., Sect. A **562**, 198 (2006).

[47] R. Cooper, L. Garrison, H. O. Meyer, T. Mikev, L. Rebenitsch, and R. Tayloe, arXiv:1110.4432.

[48] E. Kolbe and K. Langanke, Phys. Rev. C **63**, 025802 (2001).

[49] W. Verkerke and D. P. Kirkby, eConf C0303241, MOLT007 (2003).

[50] D. Akimov et al. (COHERENT Collaboration), arXiv:2006.12659.

[51] J. Dorenbosch et al. (CHARM Collaboration), Phys. Lett. **180B**, 303 (1986).

[52] http://energy.gov/downloads/doe-public-access-plan.

[53] See Supplemental Material at http://link.aps.org/supplemental/10.1103/PhysRevLett.126.012002 for additional details about the analysis.